Electronic Supplementary Material (ESI) for ChemComm.

Dynamic selection of high-affinity aptamer using a magnetically activated continuous deflection microfluidic chip

Ke-Zhu Yang, Meng Wang, Ming-Yue Gao, Yong-Tao Wang, and Zhi-Ling Zhang*

College of Chemistry and Molecular Sciences, Wuhan University, Wuhan, 430072, People's Republic of China. E-mail: zlhang@whu.edu.cn

** Corresponding author*

Experimental Section

Materials and chemicals

Streptavidin (SA) was purchased from VWR Life Science. N-Hydroxysuccinimide (NHS), 1-(3-Dimethylaminopropyl)-3-ethylcarbodiimide hydrochloride (EDC), Concanavalin A-biotin conjugate (ConA-biotin) and Bovine serum albumin (BSA) were purchased from Sigma-Aldrich. 2×Hiff® Robust PCR Master Mix was purchased from Yesen. Potato Dextrose Broth (PDB) was purchased from Bio-way technology. Crystal Violet Staining Solution (CVSS) was purchased from Beyotime. The yeast strains *Candida albicans* (CCTCC AY 93025), *Saccharomyces cerevisiae* (CCTCC AY 93135), *Staphylococcus aureus* (CCTCC AB 91093), and *Escherichia coli* (CCTCC AB 91112) were purchased from China typical culture preservation Center. The yeast strain *Pseudomonas aeruginosa* (BNCC 337005) was purchased from the BeNa Culture Collection. The initial library of the whole SELEX process consisted of a central random sequence of 40 nucleotides (nt) flanked by 20 nt primer hybridization sites for PCR (5′-Alexa Fluor 488-AGCGTCGAATACCACTACAG(N40)CTAATGGAGCTCGTGGTCAG-3′). The forward primer (FP) was labeled with Alexa Fluor 488 at the 5′-end (5′-Alexa Fluor 488-AGCGTCGAATACACTACAG-3′), the reverse primer (RP) was labeled with biotin at the 5′-end (5′-biotin-CTGACCACGAGCTCCATTAG-3′). All these oligonucleotides were synthesized and HPLC purified by Sangon Biotechnology. The 100 bp ssDNA ladder was purchased from Sangon Biotechnology. Indium tin oxide with a resistance of 10 Ω was purchased from LaiBao. AZ9260 photoresist and SU8-2050 photoresist were purchased from AZ Electronic Materials. Polydimethylsiloxane (PDMS, RTV615A + RTV615B) was purchased from GE Toshiba Silicones.

The binding buffer used in the experiment was composed of the following: 20 mM Hepes, 150 mM NaCl, 2 mM KCl, 2 mM $MgCl_2$, and 2 mM $CaCl_2$ (pH 7.4). The washing buffer consisted of a binding buffer plus 0.05% Tween-20.

Absorbance was measured by a UV-Vis spectrophotometer (UV-2550, Shimadzu). Fluorescence intensity was measured by a fluorescence spectrophotometer (Nanolog, HORIBA Jobin Yvon). Hydrodynamic size and zeta potential were measured by a dynamic light scattering instrument (ZetaSizer Nano ZEN3600 Malvern). Microscopic image was taken by an inverted fluorescence microscope (TE2000-U, Nikon) equipped with a charge-couple device (CCD) (Nikon DS-Ril).

Fabrication of the magnetically activated continuous deflection chip

As shown in Figure. S1, the MACD chip structure from bottom to top was three permanent magnets, an ITO glass substrate with the nickel strip, and a layer of PDMS to encapsulate the nickel strip and the fluid channel. Figure. S2 provided the CAD image of the fluid channel and nickel strip. The fluid channel consisted of three inlets, a 1.5-mm-side main channel, and two outlets. The width of the strip was 100 μm and the spacing between the nickel strip was 100 μm. The angles between the strip and X-axis direction from left to right were 10°, 3°, and 5°, respectively. The fabrication of the MACD chip was shown in Figure. S3. In brief, the fluidic channel was fabricated using an 80 μm thick negative SU8 2050 photoresist. The nickel structure was fabricated using positive AZ9260 photoresist. Then the nickel structure was electroplated on the place that was not covered by the photoresist. After ethanol washed away the excess photoresist, PDMS was used to encapsulate the nickel structure. Finally, the fluidic channel layer and PDMS layer were cleaned by plasma for 2

min and then irreversibly bonded together.

Numerical simulation of the microregion of the chip

COMSOL Multiphysics software was used to simulate the distribution of microregion magnetic flux density and magnetic field gradient ($|(B\cdot\nabla)B|$) in the chip. The residual flux density of the permanent magnet was 1.17 T, the relative magnetic permeability of the nickel strip was 200, and the model relative magnetic permeability of air was 1.

Preparation of MNs-bacteria complex

Magnetic nanospheres (MNs) were fabricated by layer-by-layer method.[1] The SA protein was chemically conjugated to magnetic beads by two-step activation with EDC and NHS. Bacteria-MNs complex was prepared in two steps. Biotinylated bacteria were obtained by incubating bacteria with ConA-biotin in the first step. MNs-bacteria complex was obtained by incubating biotinylated bacteria with MNs-SA in the second step.

To explore whether the reaction could be carried out at a continuous flow rate using the MACD chip, the MNs-SA solution, biotin solution (5′-Alexa Fluor 488-AGCGTCGAATACACTACAG-biotin-3′), and 1×PBS (pH 7.2) were pumped into the chip at 2 μL/min for reacting 1.5 h. The collected reactants were observed under an inverted fluorescence microscope.

Optimization of the selection condition

The stringency of the condition was increased by lowering the target concentration in dynamic selection. Pretreated DNA was obtained by the following steps: heated at 95 ℃ for 10 min, then immediately cooled to 0 ℃ on ice for 10 min, and finally incubated for 5 min at room temperature

to form multiple spatial structures. Different numbers of bacteria (3.82×10^6, 7.64×10^6, 1.91×10^7, 3.82×10^7, 5.73×10^7, 7.64×10^7) in 200 μL binding buffer, 200 μL 50 pmol pretreated DNA library and 200 μL washing buffer were pumped into the MACD chip at 2 μL/min, respectively. The recovered products were measured by a UV spectrophotometer and a fluorescence spectrophotometer. Then the average fluorescence intensity of individual bacteria was calculated.

Selection of aptamer for *C. albicans*

MNs-*S. cerevisiae*, which was used as the negative bacteria, was pumped into the array chip at 2 μL/min. After MNs-*S. cerevisiae* was trapped in the array chip, 200 μL 200 pmol pretreated library was pumped into the chip at 2 μL/min for 2 h. The ssDNA excluded from nonspecific adsorption was collected in a reservoir. Subsequently, the positive bacteria (*C. albicans*), the ssDNA library, and the washing buffer were pumped into the MACD chip at 2 μL/min, respectively. The collected bacteria-ssDNA was measured by a fluorescence spectrophotometer. Then the bacteria-ssDNA was amplified by PCR and the 30 μL PCR mixture consisted of 1 μL 10 μM Alexa Fluor-FP, 1 μL 10 μM biotin-RP, 5 μL template, 8 μL water and 15 μL 2×Hiff® Robust PCR Master Mix. The PCR program was as the follows steps: 96 ℃ for 10 min, 25 cycles at 96 ℃ for 15 s, 56 ℃ for 30 s, 72 ℃ for 15 s, and at 72 ℃ for 5 min for an extension. Then the PCR mix was incubated with MNs-SA for 45 min at room temperature to obtain the dsDNA. The dsDNA reacted with 0.1 M NaOH to release the ssDNA and the ssDNA was purified by a 10K ultrafiltration tube to form a secondary library for the next round of selection.

Cloning and sequencing

After six rounds of selection, the fluorescence intensity did not increase obviously, the selection

was stopped. PCR products amplified by unlabeled primers were cloned. Twenty colonies were randomly selected and sequenced at the Hecegene. The sequences were analyzed by the software DNAMAN and Clustalx. The sequences with high homology were picked for affinity testing.

Measurements of binding affinity

The affinity of the selected aptamers was evaluated by the K_d value, which was measured by a fluorescence binding assay. First, the FAM-labeled aptamers were diluted to different concentrations (0, 5, 10, 25, 50, 100, 150, 200 nM) in the binding buffer. Next, the pretreated aptamers were incubated with MNs-*C. albicans* for 1 h at room temperature. After unbound sequences were removed by magnetic separation, the fluorescence intensity of the complex was measured by the K_d values by subtracting the fluorescence intensity of the initial library. The software SigmaPlot 14 was used to calculate the K_d values according to the equation: $Y = B_{max}X/(K_d + X)$. Y is the fluorescence intensity, X is the aptamer concentration and B_{max} is the saturation fluorescence intensity. The secondary structure of the aptamer was simulated using Mfold web.

Specificity measurement and the effect of aptamer on biofilms

The aptamer with the highest affinity was selected to analyze the specificity and the effect on biofilms. Pretreated FAM-labeled aptamers were incubated with different types of bacteria (such as *S. cerevisiae*, *S. aureus*, *E. coli*, and *P. aeruginosa*). The fluorescence intensity of the bacteria-aptamer was measured. To further evaluate the effect of the aptamer on the biofilm formation of *C. albicans*, pretreated aptamers were added to 96-well plates and diluted with PDB to different concentrations (200, 400, 600, 800, 1000 nM). The activated *C. albicans* were added separately to incubate for 24 h. After washing with 1×PBS (pH 7.2), 200 μL of CVSS was added and incubated

for 60 min. After washed three times with 1×PBS (pH 7.2), 200 μL of acetic acid was added.

Results and Discussion

S.1 Structure of the MACD chip

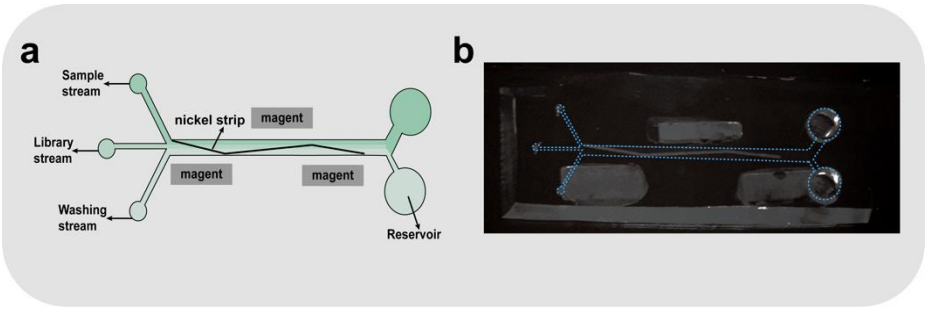

Figure. S1 (a) Image of the MACD chip. (b) Photograph of the MACD chip

S.2 CAD picture

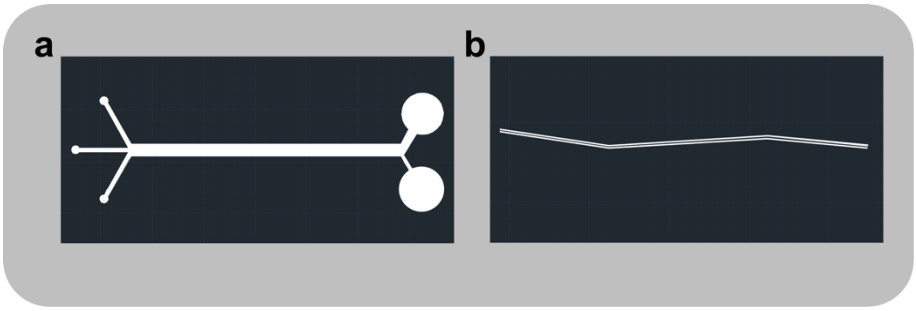

Figure. S2 CAD pictures of the (a) fluid channel and (b) nickel strip.

S.3 Fabrication of the MACD chip

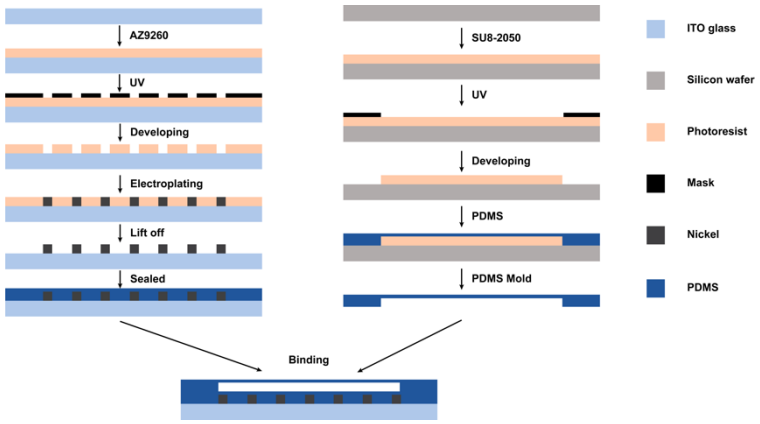

Figure. S3 Schematic diagram of the fabrication procedure for the MACD chip.

S.4 Laminar flow simulation

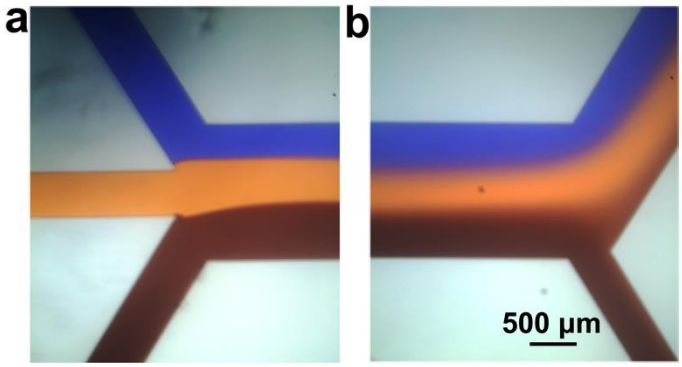

Figure. S4 Image of red, blue, and black ink simulating laminar flow in the MACD chip of (a) inlet and (b) outlet. The scar bar is 500 μm.

S.5 Accumulation of MNs at the end of the nickel strip

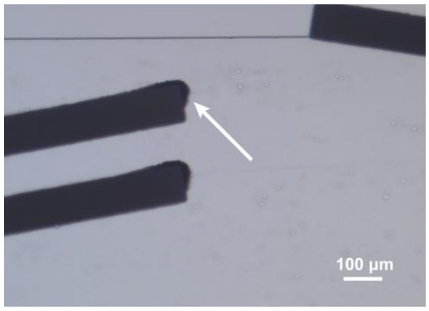

Figure. S5 Image of MNs at the end of the nickel strip in the intermittent chip. The scar bar is 100 μm.

S.6 Numerical simulation

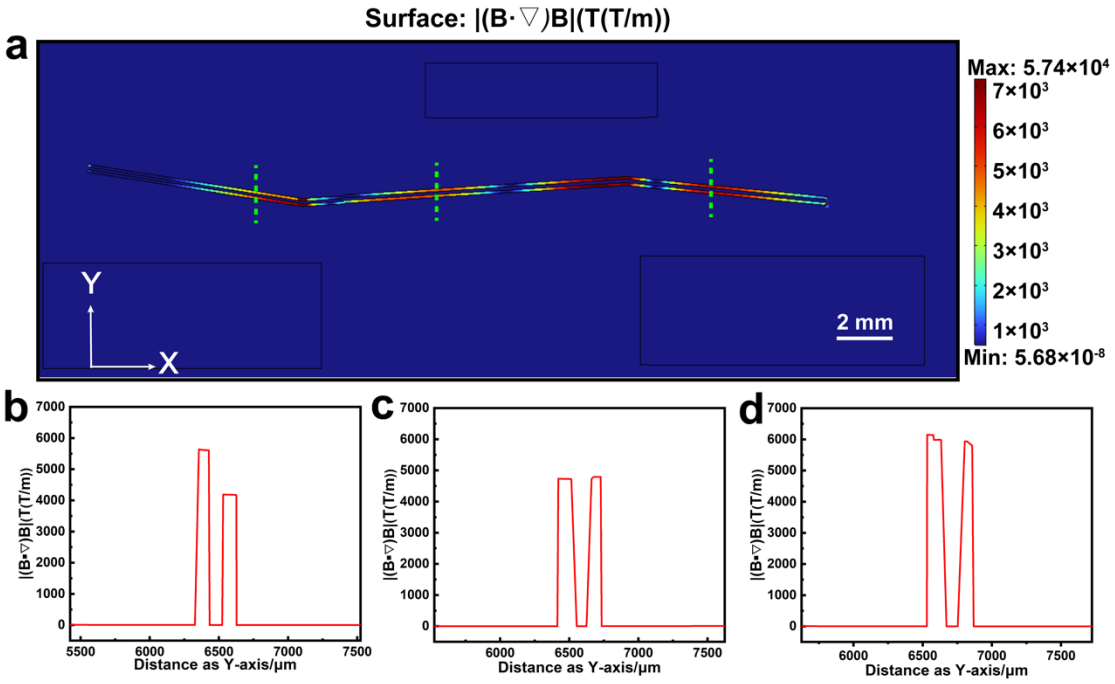

Figure. S6 (a) Simulated color map of |(B·∇)B| in the MACD chip. Numerical simulation results of |(B·∇)B| vs the distance (b-d) along the green lines in the Y-axis direction. The scar bar is 2 mm.

S.7 Stress analysis of MNs

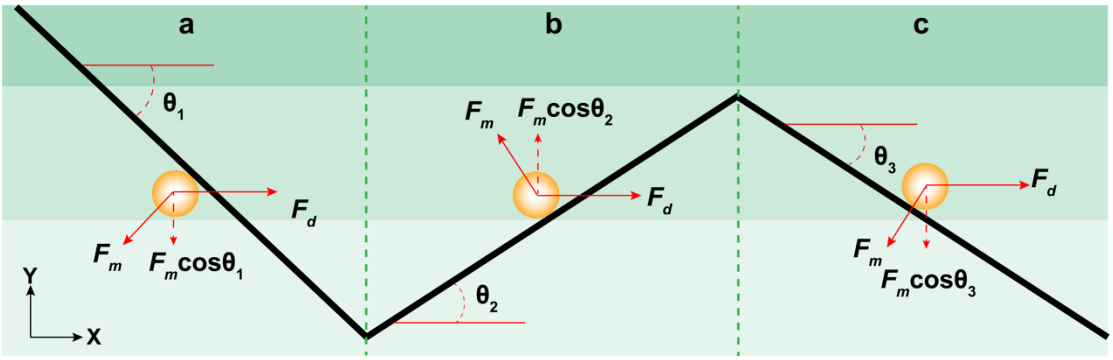

Figure. S7 Stress analysis of MNs in different regions of the nickel strip.

MNs were mainly affected by hydrodynamic drag force (F_d) and magnetic force (F_m) in the microregion. F_d made MNs move forward in the X-axis. F_m on MNs could be calculated on the equation: $F_m = (\Delta\chi \cdot V_m \cdot (B\cdot\nabla)B)/\mu_0$. $\Delta\chi$ is the difference of the magnetization coefficient between

MNs and the surrounding medium, V_m is MNs volume, and μ_0 is vacuum permeability ($4\pi\times10^{-7}$, $H\cdot m^{-1}$). $\Delta\chi$ was taken a value of 1.52 to calculate F_m.[2] The F_m on MNs was on the order of nanonewtons MNs. Therefore, the component of F_m in the Y-axis direction ($F_m\cos\theta$) was large enough to make MNs move in the X-axis.

S.8 Fluorescence trace pattern of MNs

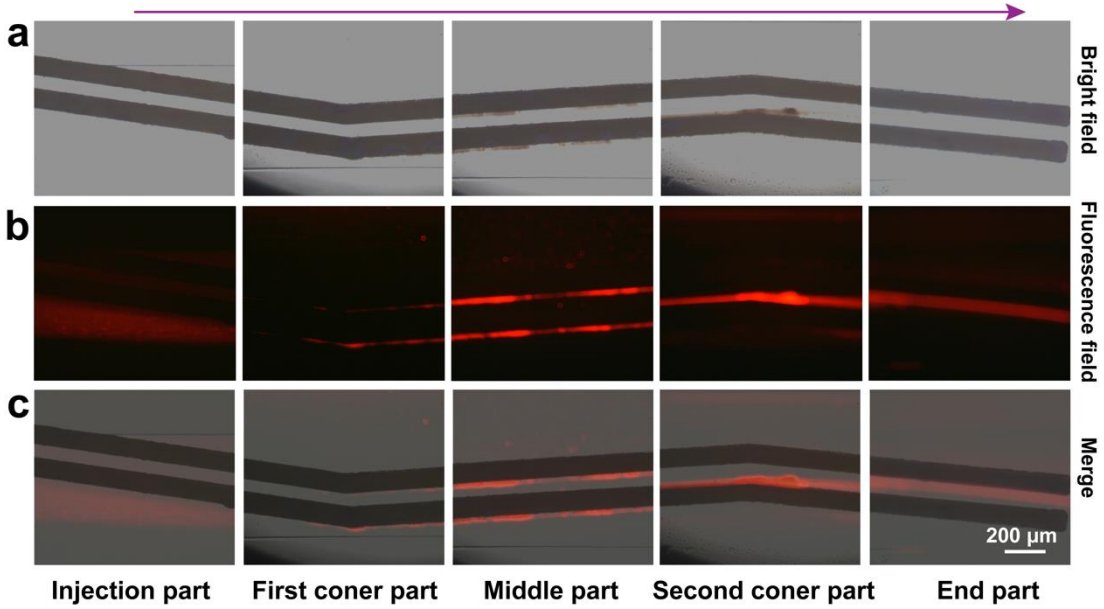

Figure. S8 Images taken in five different parts of the deflection zone in (a) bright field, (b) fluorescence field, and (c) merge. The purple arrow indicates the direction of the fluid. The scar bar is 200 μm.

S.9 The combination feasibility of the MACD chip

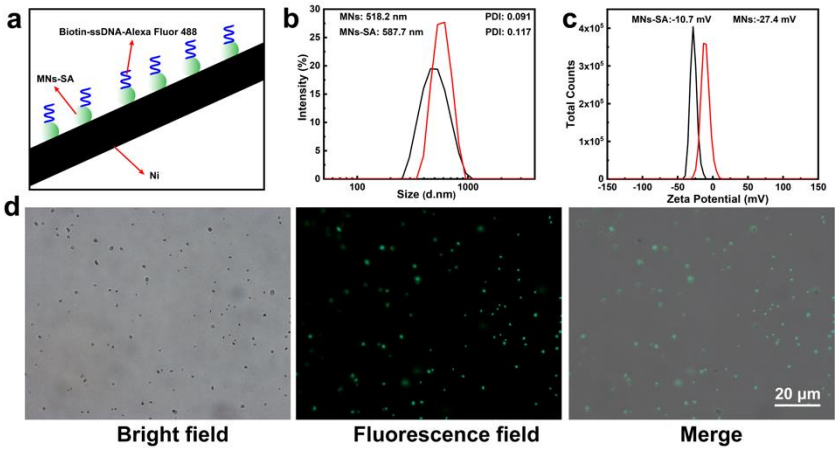

Figure. S9 (a) Binding diagram of the MACD chip. (b) Hydrodynamic diameter distribution of MNs and MNs-SA. (c) Zeta (ζ) potential characterization of MNs and MNs-SA. (d) Microscope picture of MNs-SA after binging in the MACD chip. The scar bar is 20 μm.

S.10 Preparation of MNs-bacteria

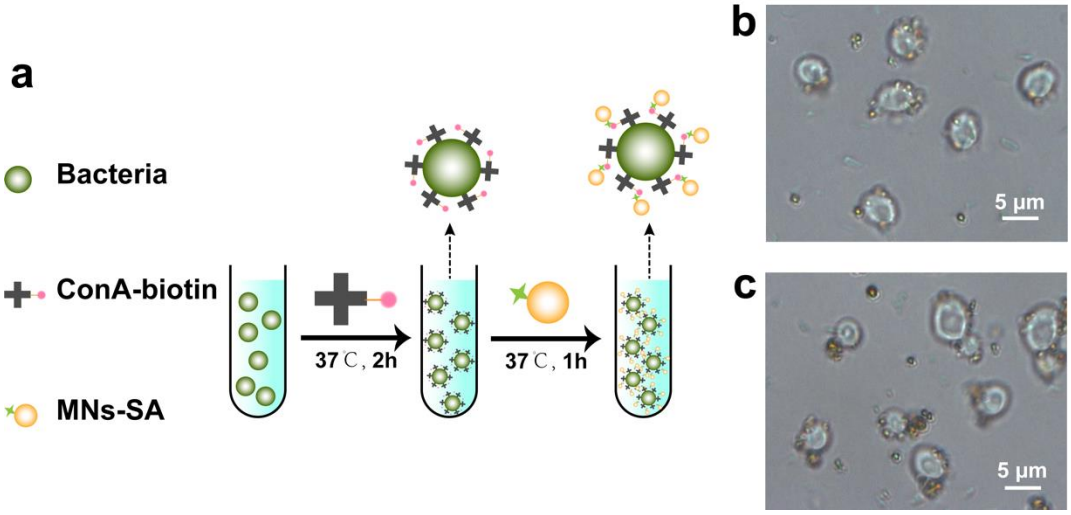

Figure. S10 (a) Schematic representation of the principle of MNs-SA coupled with bacteria. Image of (b) MNs-*S. cerevisiae* complex and (c) MNs-*C. albicans* complex. The scar bar is 5 μm.

S.11 Optimization of ConA-biotin and MNs-SA

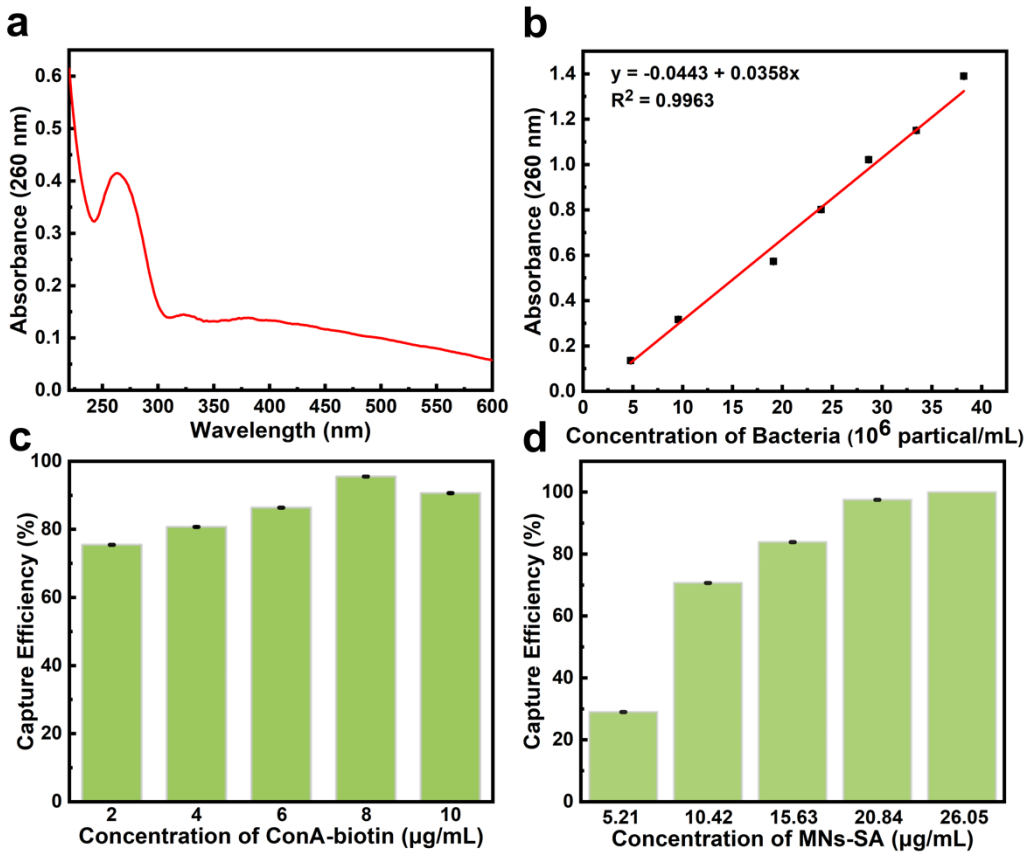

Figure. S11 (a) UV absorption of *C. albicans* at 260 nm. (b) Standard curve between absorbance and concentration (n = 3). Optimization of the amount of (c) ConA-biotin and (d) MNs-SA (n = 3).

S.12 Fluorescence trace pattern of MNs-*C. albicans*

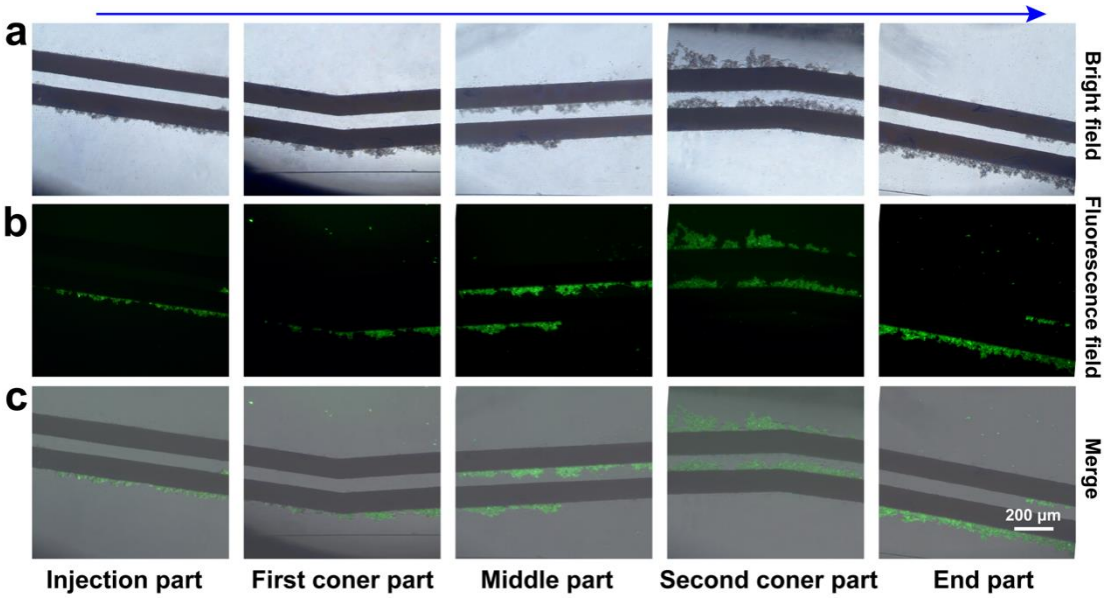

Figure. S12 Images taken in five different parts of the deflection zone in (a) bright field, (b) fluorescence field, and (c) merge. The direction of the blue arrow represents the direction of fluid flow. The scar bar is 200 μm.

S.13 Continuous elution of low-affinity sequences.

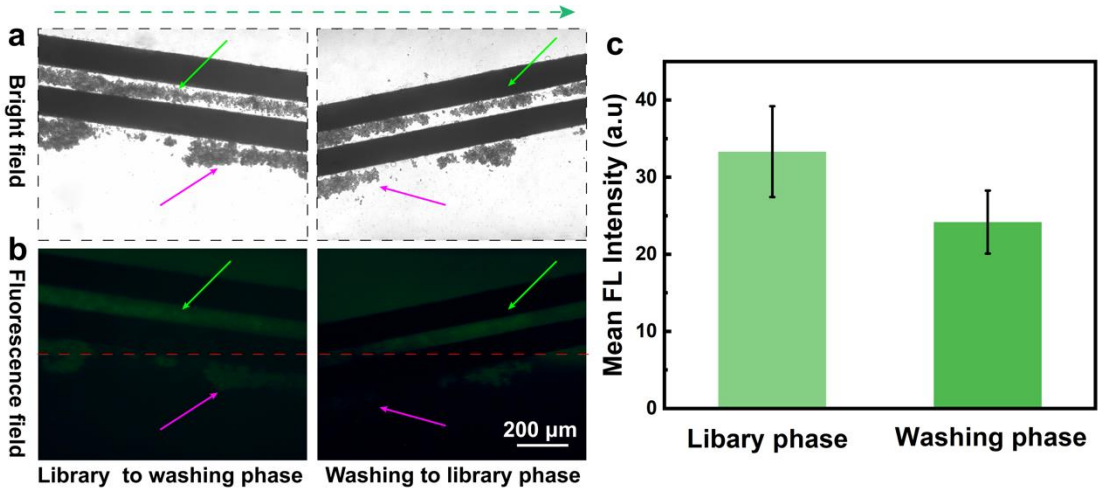

Figure. S13 Microscopes pictures of *C. albicans* moving from different phases were taken in (a) bright field, and (b) fluorescence field. The red dashed line represented the boundary dividing the library phase and the washing phase. Green arrows indicated the location of *C. albicans* in the library phase and magenta arrows indicated the location of *C. albicans* in the washing phase The green dashed arrow represented the direction of fluid motion. The scar bar is 200 μm. (c) Mean fluorescence intensity of *C. albicans* in the library phase and the washing phase, respectively (n=16).

The fluorescence intensity of bacteria moving from different phases was monitored on the inverted fluorescence microscope. It could be found that the fluorescence intensity of *C. albicans* decreased when *C. albicans* moved from the library phase to the washing phase (Fig S13a,b). To quantitatively compare the fluorescence binding intensity between the library phase and the washing phase, the mean fluorescence intensity values of 16 images were quantified. According to the results, the mean fluorescence intensity value of bacteria in the library phase was significantly higher than that in the washing phase (Fig S13c). Thus, the low-affinity sequences were eluted when the washing phase was present.

S.14 Binding fluorescence of positive and negative selection

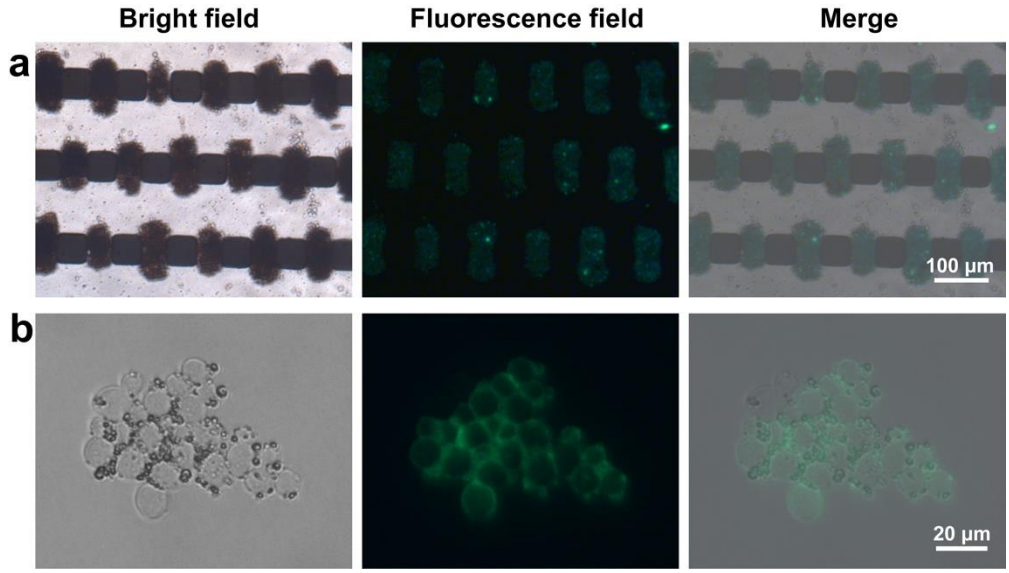

Figure. S14 (a) Microscopic picture of the negative selection unit in bright field, fluorescence field and merge. The scar bar is 100 μm. (b) Microscopic picture of the positive selection in bright field, fluorescence field, and merge. The scar bar is 20 μm.

S.15 Preparation of secondary libraries

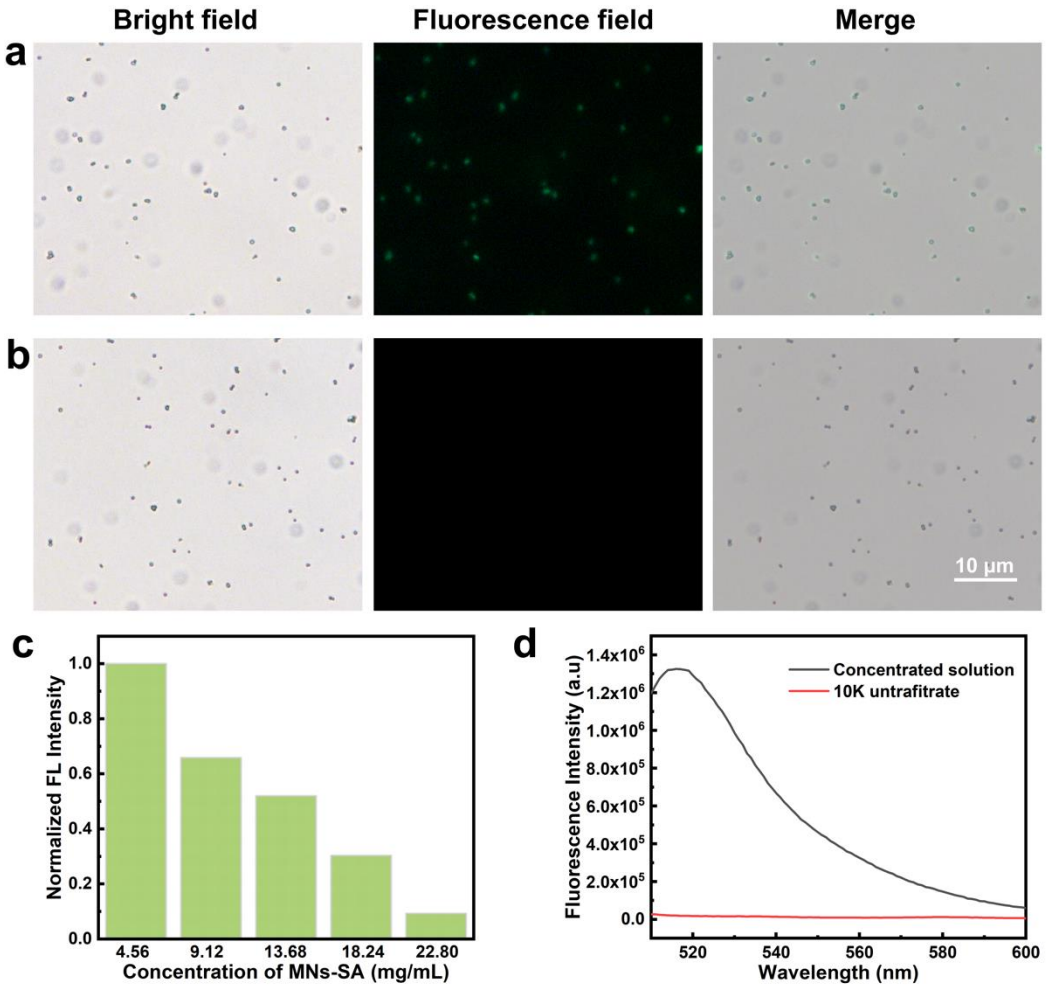

Figure. S15 (a) Image of amplification products captured by MNs-SA. (b) Microscopic image of MNs-SA-biotin-DNA treated with NaOH. (c) Optimization of MNs-SA amount during capturing the biotin-modified PCR products. (d) Purification of the evolved libraries by a 10K ultrafiltration tube. The scar bar is 10 μm.

S.16 Analysis of homology

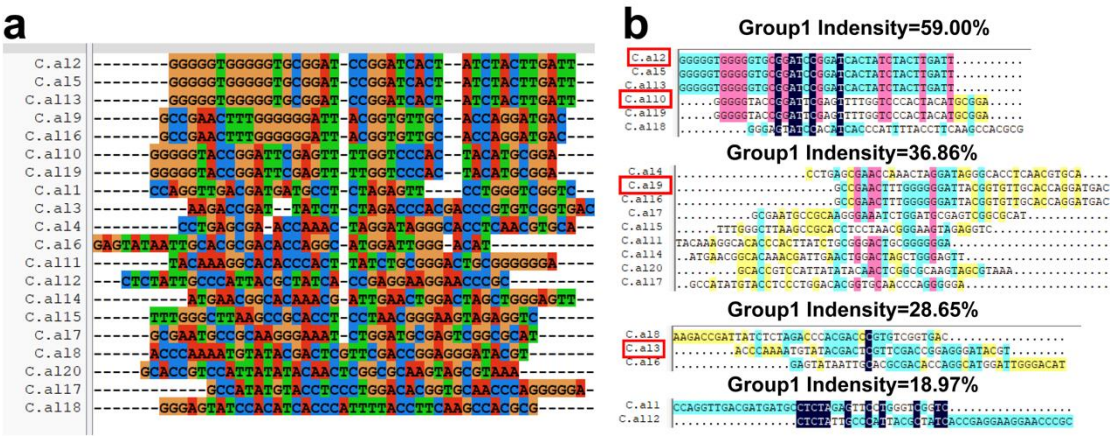

Figure. S16 (a) Sequence analysis by Clustalx software. (b) Analysis of homology by DNAMAN software.

S.17 The *K*d value of aptamers for different types of bacteria

Table S1 The K_d value of aptamers for different types of bacteria

Target	K_d value (nM)	Sequence (5′→3′)	References
Shigella dysenteriae	23.47 ± 2.48	CGGAACTAGCGTTTAAATGCCAGGAC TGAAGTAGGCAGGG	3
Streptococcus pyogenes	7 ± 1	CACACACGGAACCCCGACAACATACA TACGGTGAGGGTGG	4
Staphylococcus aureus	43.3 ± 3.0	GGGACAGGAGTGCGCTGCTCCCC	5
Vibrio alginolyticus	14.31 ± 4.26	TCGGTCGGGTGGTTGGGGTGGGTGGT CGGTTTTTAAGCTGTGTCATTGTC	6
Legionella pneumophila	12.98 ± 3.24	TCGGTAAGGGCAGTCTTAGCGTGGTT CCATCTGTACCGAAGCCGT	7
Pseudomonas aeruginosa	28.47	CCATCCACACTCCGCAAGTGGGGAGG GGAGAGACGACGATCCTGTGGGTTTT CTGCAGTGAGTCCTGTTTTCGACTTAT TGCGTCGGCTGCCTCTACAT	8
Helicobacter pylori	19.3 ± 3.2	CCAGGAGGACCCTATTCTCGTGTATC GACGAGATCCAGTG	9
Bacillus anthracis	11.0 ± 2.7	CGAGGGAGACGCGAACCTTCTCGCCT TGGG	10
Escherichia coli O157:H7	10.30	TGGTCGTGGTGAGGTGCGTGTATGGG TGGTGGATGAGTGTGTGGC	11
Candida albicans	79.76	GCGGAATTCGAACAGTCCGAGCCCAC ACGTGTGAGAAGGGTGTTATCATGTAT TTCGTGTTCCTTTCGTCATTCCTTTGT CTGGGGTCAATGCGTCATAGGATCCC GC	12
Candida albicans	-	AGCCCUCAACCCAGACACCCCCAAC CUUCCUCGCCCCCCC	13

REFERENCES

1 R. J. S. Derks, A. Dietzel, R. Wimberger-Friedl and M. W. J. Prins, *Microfluid. Nanofluid.,* 2007, **3**, 141–149.

2 C.Y. Wen, L.L. Wu, Z.L. Zhang, Y.L. Liu, S.Z. Wei, J. Hu, M. Tang, E.Z. Sun, Y.P. Gong, J. Yu and D.W. Pang, *ACS Nano*, 2014, **8**, 941–949.

3 N. Duan, X. Ding, S. Wu, Y. Xia, X. Ma, Z. Wang and J. Chen, *J. Microbiol. Meth.*, 2013, **94**, 170–174.

4 C. L. A. Hamula, H. Peng, Z. Wang, G. J. Tyrrell, X.F. Li and X. C. Le, *Methods*, 2016, **97**,

51–57.
5 M. I. A. De Melo, P. Da Silva Cunha, I. M. Ferreira and A. S. R. De Andrade, *Mol. Biol. Rep.*, 2023, **50**, 157–165.
6 Q. Yu, M. Liu, H. Su, H. Xiao, S. Wu, X. Qin, S. Li, H. Mi, Z. Lu, D. Shi and P. Li, *J. Fish Dis.*, 2019, **42**, 851–858.
7 L. Xiong, M. Xia, Q. Wang, Z. Meng, J. Zhang, G. Yu, Z. Dong, Y. Lu and Y. Sun, *Biotechnol. Lett.*, 2022, **44**, 777–786.
8 M. Zhao, W. Li, K. Liu, H. Li and X. Lan, *PLoS ONE*, 2019, **14**, e0212041.
9 H. Wu, L. Gu, X. Ma, X. Tian, S. Fan, M. Qin, J. Lu, M. Lyu and S. Wang, *ACS Omega*, 2021, **6**, 3771–3779.
10 M. Lahousse, H.C. Park, S.C. Lee, N.-R. Ha, I.P. Jung, S. R. Schlesinger, K. Shackelford, M.Y. Yoon and S.K. Kim, *Arch. Biochem. Biophys.*, 2018, **646**, 16–23.
11 X. Yu, F. Chen, R. Wang and Y. Li, *J. Biotechnol.*, 2018, **266**, 39–49.
12 X.L. Tang, Y. Hua, Q. Guan and C.H. Yuan, *Eur. J. Clin. Microbiol. Infect. Dis.*, 2016, **35**, 587–595.
13 B. M. Bachtiar, C. Srisawat and E. W. Bachtiar, *MicrobiologyOpen*, 2019, **8**, e00812.